APPLIED GEOPHYSICS, Vol.10, No.4 (December 2013), P. 384-396, 7 Figures.
DOI: 10.1007/s11770-013-0400-6

# Stability of finite difference numerical simulations of acoustic logging-while-drilling with different perfectly matched layer schemes*

Wang Hua[1,2], Tao Guo[1♦], Shang Xue-Feng[2], Fang Xin-Ding[2], and Daniel R Burns[2]

**Abstract**: In acoustic logging-while-drilling (ALWD) finite difference in time domain (FDTD) simulations, large drill collar occupies, most of the fluid-filled borehole and divides the borehole fluid into two thin fluid columns (radius ~27 mm). Fine grids and large computational models are required to model the thin fluid region between the tool and the formation. As a result, small time step and more iterations are needed, which increases the cumulative numerical error. Furthermore, due to high impedance contrast between the drill collar and fluid in the borehole (the difference is >30 times), the stability and efficiency of the perfectly matched layer (PML) scheme is critical to simulate complicated wave modes accurately. In this paper, we compared four different PML implementations in a staggered grid finite difference in time domain (FDTD) in the ALWD simulation, including field-splitting PML (SPML), multiaxial PML(M-PML), non-splitting PML (NPML), and complex frequency-shifted PML (CFS-PML). The comparison indicated that NPML and CFS-PML can absorb the guided wave reflection from the computational boundaries more efficiently than SPML and M-PML. For large simulation time, SPML, M-PML, and NPML are numerically unstable. However, the stability of M-PML can be improved further to some extent. Based on the analysis, we proposed that the CFS-PML method is used in FDTD to eliminate the numerical instability and to improve the efficiency of absorption in the PML layers for LWD modeling. The optimal values of CFS-PML parameters in the LWD simulation were investigated based on thousands of 3D simulations. For typical LWD cases, the best maximum value of the quadratic damping profile was obtained using one $d_0$. The optimal parameter space for the maximum value of the linear frequency-shifted factor ($\alpha_0$) and the scaling factor ($\beta_0$) depended on the thickness of the PML layer. For typical formations, if the PML thickness is 10 grid points, the global error can be reduced to <1% using the optimal PML parameters, and the error will decrease as the PML thickness increases.
Keywords: PML schemes, FD simulation, LWD acoustic

## Introduction

Acoustic logging-while-drilling (ALWD) can provide important information about formations during drilling operations (Aron et al., 1997; Wang et al., 2009). However, because the drill collar occupies most of the fluid-filled borehole and divides the borehole

Manuscript received by the Editor June 17, 2013; revised manuscript received October 30, 2013.
*This study was supported by NSFC (No.41174118), one of the major state S &T special projects (No.2008ZX05020-004), a Postdoctoral Fellowship of China (No.2013M530106) and China Scholarship Council (No.2010644006).
1. State Key Laboratory of Petroleum Resource and Prospecting, China University of Petroleum, Beijing 102249, China.
2. Earth Resource Laboratory, Massachusetts Institute of Technology, Cambridge, MA, USA, 02139.
♦Corresponding author: Tao Guo (Email: taoguo@vip.sina.com)

fluid into two thin fluid columns (Byun and Toksoz, 2003), the receiving wave-field is different from that in acoustic wire-line logging. Therefore, the wave-field characteristics in ALWD need to be well understood to obtain accurate formation properties.

Numerical simulations can help us understand the characteristics of the complex LWD wave field. Many different numerical methods have been used in seismic wave propagation simulation, such as the discrete wave number method (Bouchon and Aki, 1977), the finite difference method (Alterman and Karal, 1968; Madariaga, 1976; Virieux, 1984; Virieux, 1986), the finite element method (Lysmer and Drake, 1972; Marfurt, 1984), the boundary element method (Kawase, 1988), the pseudo-spectral method (Carcione, 1994; Tessmer and Kosloff, 1994), and the spectral element method (Cohen et al., 1993).

Among these, the discrete wave number method (DWM) (Cheng and Toksoz, 1981; Schmitt and Bouchon, 1985; Kurkjian and Chang, 1986; Wang and Tao, 2011), the finite difference in time domain (FDTD) (Cheng, 1994; Wang and Tang, 2003a; Wang and Tang, 2003b; Tao et al., 2008; Wang et al., 2009), and the finite element method (FEM) (Matuszyk and Torres-Verdin, 2011; Wang et al., 2013) are commonly used to simulate the acoustic logging wave field. The DWM is numerically fast, but is difficult to implement for non-axial symmetric models, such as tool isolation design (Chen et al., 1998; Wang et al., 2009) and acoustic LWD tool eccentricity (Huang, 2003). Furthermore, the FDTD and FEM can be numerically demanding for large 3D models, but can handle general spatial variations of elastic properties. However, the FEM is difficult to program and the computational cost is several times higher than FDTD (Wang et al., 2012).

The FDTD implementations include computational domain boundaries that will inevitably bring the reflected energy back into the computational domain, and then contaminate the signal. To avoid the artificial reflection from computational domain boundaries, many methods have been developed: nonreflecting plane boundary condition (Smith, 1974), absorbing boundary conditions (ABCs) (Clayton and Engquist, 1977; Higdon, 1990), absorbing boundary layers (Cerjan et al., 1985; Sochacki et al., 1987), and transparent boundary (Zhu, 1999). The perfectly matched layer (PML) methods (Berenger, 1994; Chew and Weedon, 1994) were initially developed for Maxwell's equation problems. The idea of PML is to add layers of absorbing material outside of the computational domain, which can exponentially attenuate the entering energy and attenuate again when the energy is reflected back from the outer boundary of the PML. If the layer is large enough, the energy will be completely absorbed in the layer. PML has since been introduced into seismic wave propagation simulation (Chew and Liu, 1996; Collino and Tsogka, 2001; He, et al., 2013) and borehole wave propagation simulation (Kuzuoglu and Mittra, 1996; Wang and Tang, 2003a and 2003b; Tao et al., 2008; Guan, et al., 2009; Wang et al., 2009). The PML method later also evolved into several different types, from field-splitting PML (SPML) (Berenger, 1994; Collino and Tsogka, 2001) to complex frequency shifted PML (CFS-PML) (Kuzuoglu and Mittra, 1996; Roden and Gedney, 2000; Komatitsch and Martin, 2007).

Unlike wire-line acoustic logging models, in acoustic LWD FDTD simulations, large drill collar occupies most of the fluid-filled borehole and divide the borehole fluid into two thin fluid columns (radius ~27 mm). Fine grids and large computational models are required to model the thin fluid region between the tool and the formation. As a result, small time step and more iterations are needed, which increases the cumulative numerical error. In addition, the high impedance contrast (the difference is >30 times) between the fluid and tool requires a high efficiency method to capture the rich and subtle features in the late arrivals. Because of these challenges, efficient computational boundary conditions are critical to allow realistic simulations of ALWD problems with FDTD, which will be very different from seismic wave propagation simulations.

In this paper, FDTD simulations of ALWD cases were compared completely and systematically for four different PML implementations (SPML, M-PML, NPML (non-splitting PML), and CFS-PML). The merits and demerits of the different PML methods were compared, and the optimal parameters of CFS-PML in typical ALWD cases were explored.

## Elastic wave equation implementation for ALWD simulations

Acoustic LWD can be modeled by placing a drill collar in a fluid-filled borehole with sources and receivers embedded on the outer edge of the drill collar. The model configuration and vibration modes of the sources are illustrated in Figure 1. Figure 1a and 1b are the top view of the model. As Figure 1a and 1b show, the drill collar occupies most of the fluid-filled borehole, and the "+" and "−" sings represent the loading pattern of the sources,

with Figure 1a representing a monopole source and 1b a quadrupole source. The explosive sources are loaded at the stress grids closest to the collar. The vibration modes of the sources are indicated by the arrows. Although the FD in the cylindrical coordinate system is better than that in the Cartesian coordinate system for the simulation of the wave field in the LWD, the FD in the Cartesian coordinates system is used in this paper for the consideration of the simulation for a larger model in later. Figure 1c is a schematic of the $x$–$z$ cross-section, where $x$ is along the horizontal (radial) direction, and $z$ is the vertical direction. The schematic also shows the arrangement of the sources and receivers. The tool and model parameters are listed in Table 1.

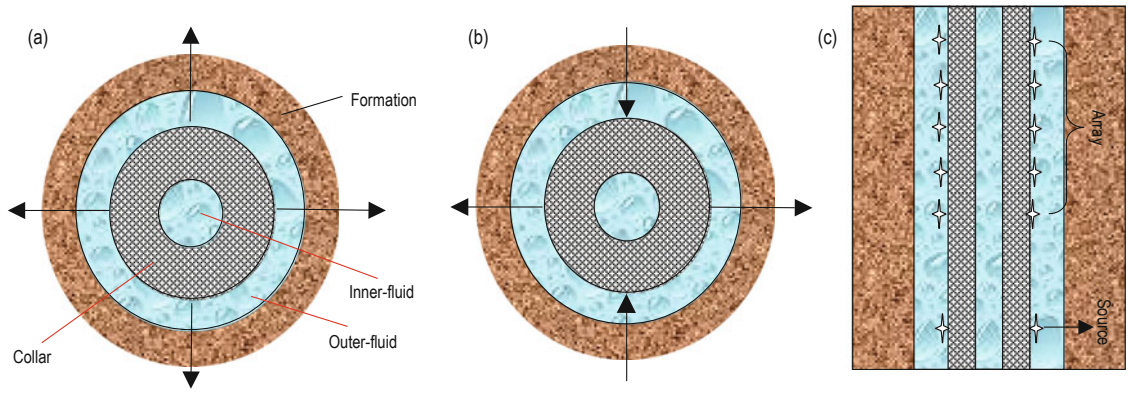


**Fig.1 Schematic of model and the location of source and receivers.**
(a) Top view of the monopole source model.Vibration modes of sources are indicated by arrows. (b) Top view of the quadrupole source model. Vibration modes of sources are indicated by arrows. (c) Schematic of x–z cross-section. x is along the horizontal direction, and z is vertical direction.

**Table 1 Model parameters**

| | $V_p$ (m·s$^{-1}$) | $V_s$ (m·s$^{-1}$) | Density (g·cm$^{-3}$) | Radius (mm) |
|---|---|---|---|---|
| Inner fluid | 1470 | — | 1.00 | 27 |
| Drill collar | 5860 | 3130 | 7.85 | 90 |
| Outer fluid | 1470 | — | 1.00 | 117 |
| Sandstone | 3927 | 2455 | 2.32 | ∞ |
| Limestone | 6500 | 3800 | 2.71 | ∞ |
| Mudstone | 2100 | 510 | 2.00 | ∞ |

Note: $V_p$ is P-wave velocity and $V_s$ is S-wave velocity.

In the FD simulations of acoustic logging, we used the velocity–stress formulation of the elastic wave equation (Zhang and Shen, 2010):

$$\frac{\partial \mathbf{v}}{\partial t} = \frac{1}{\rho}\nabla \cdot \boldsymbol{\sigma}, \tag{1a}$$

$$\frac{\partial \boldsymbol{\sigma}}{\partial t} = \mathbf{c} : [\nabla \mathbf{v} + (\nabla \mathbf{v})^T]/2, \tag{1b}$$

where $v$ is the particle velocity vector, $\boldsymbol{\sigma}$ is the stress tensor, $\rho$ is the density of medium, and $\mathbf{c}$ is the stiffness tensor.

## Classical perfectly matched layer (PML)

Consider the plane wave solution of wave equation (1) in Cartesian coordinates $(x, y, z)$: $\exp[-i(k_x x + k_y y + k_z z - \omega t)]$, and using the $x$ coordinate as an example, a complex stretch factor $S_x = 1 + d_x(x)/(i\omega)$ (Chew and Weedon, 1994; Chew and Liu, 1996) is introduced in the absorbing layer. Here the subscript $x$ of $S_x$ and $d_x$ denote the $x$ direction, $d_x(x)$ is the damping function: $d_x(x) = \partial \gamma_x/\partial x\,(\gamma_x > 0)$, and $\omega$ is angular frequency. In the absorbing layer, $x$ will be replaced by $x' = x + \gamma_x/(i\omega)$, and the solution becomes $\exp[-i(k_x x + k_y y + k_z z)]\exp(-k_x \gamma/\omega)$. In such a configuration, the incident plane wave along the $x$ direction can be exponentially attenuated in the PML region.

## Split-field perfectly matched layer (SPML)

There are many methods for implementing the PML in an elastic wave propagation simulation. SPML is one of the methods that avoids the convolution operation. The detail of the method is as follows. Using the velocity in $x$ direction in governing equation (1a), the expression in the frequency domain is:

$$i\omega\rho V_x = \frac{\partial t_{xx}}{\partial x} + \frac{\partial t_{yx}}{\partial y} + \frac{\partial t_{zx}}{\partial z}, \tag{2}$$

where the terms $V_x$, $t_{xx}$, $t_{yx}$, and $t_{zx}$ are the expressions in the frequency domain of $v_x$, $\sigma_{xx}$, $\sigma_{yx}$, and $\sigma_{zx}$.

When the complex stretch factor is introduced, the space derivatives $\partial/\partial x$, $\partial/\partial y$, and $\partial/\partial z$ are replaced by $\partial/\partial x' = \partial/\partial x \cdot 1/s_x$, $\partial/\partial y' = \partial/\partial y \cdot 1/s_y$, and $\partial/\partial z' = \partial/\partial z \cdot 1/s_z$,

respectively, in the complex stretch plane.

Equation (2) can then be expressed as follows (Zhang and Shen, 2010):

$$i\omega\rho V_x = \frac{1}{S_x(x)}\frac{\partial t_{xx}}{\partial x} + \frac{1}{S_y(y)}\frac{\partial t_{yx}}{\partial y} + \frac{1}{S_z(z)}\frac{\partial t_{zx}}{\partial z}. \quad (3)$$

To avoid a convolution operation, each velocity and stress component is split further into parallel and perpendicular components with respect to the coordinate directions (Berenger, 1994; Collino and Tsogka, 2001; Tao et al., 2008; Wang et al., 2009). For example, $V_x$ can be split into three parts: $V_x = V_{xx} + V_{xy} + V_{xz}$, and equation (3) can then be expressed as follows:

$$i\omega\rho V_{xx} = \frac{1}{S_x(x)}\frac{\partial t_{xx}}{\partial x},$$

$$i\omega\rho V_{xy} = \frac{1}{S_y(y)}\frac{\partial t_{yx}}{\partial y},$$

$$i\omega\rho V_{xz} = \frac{1}{S_z(z)}\frac{\partial t_{zx}}{\partial z}. \quad (4)$$

The transformations into time domain become:

$$\frac{\partial v_{xx}}{\partial t} + d_x v_{xx} = \frac{1}{\rho}\frac{\partial \sigma_{xx}}{\partial x},$$

$$\frac{\partial v_{xy}}{\partial t} + d_y v_{xy} = \frac{1}{\rho}\frac{\partial \sigma_{yx}}{\partial y},$$

$$\frac{\partial v_{xz}}{\partial t} + d_z v_{xz} = \frac{1}{\rho}\frac{\partial \sigma_{zx}}{\partial z}. \quad (5)$$

Here, we give the implantation of SPML in the 2D staggered grid FD. Figure 2 shows the schematic of a 2D model with a PML thickness of two grid cells and a rectangular computational domain of 10 grid cells on each side. To make sure the result is exactly symmetrical to the center of the model, we only considered the two dashed-line domains: the region surrounded by the inner dashed line in the model is the computational domain and the region between the inner and outer dashed lines is the PML domain. Layers outside the model are not considered in the FD code (shown as Figure 2).

The time discrete form of equation (5) is as follows (assuming the velocity locates in the half grid of time):

$$v_{xx}^{i+\frac{1}{2}} = \frac{1-\frac{1}{2}d_x\Delta t}{1+\frac{1}{2}d_x\Delta t} v_{xx}^{i-\frac{1}{2}} + \frac{\Delta t}{\rho\left(1+\frac{1}{2}d_x\Delta t\right)}\frac{\partial \sigma_{xx}}{\partial x}\Big|^i,$$

$$v_{xz}^{i+\frac{1}{2}} = \frac{1-\frac{1}{2}d_z\Delta t}{1+\frac{1}{2}d_z\Delta t} v_{xz}^{i-\frac{1}{2}} + \frac{\Delta t}{\rho\left(1+\frac{1}{2}d_z\Delta t\right)}\frac{\partial \sigma_{xz}}{\partial z}\Big|^i,$$

$$v_x^{i+\frac{1}{2}} = v_{xx}^{i+\frac{1}{2}} + v_{xz}^{i+\frac{1}{2}}. \quad (6)$$

In the implementation of SPML with FDTD, $d_x$, $d_y$, and $d_z$ will be given different values according to the different PML domains, and only the normal components to the axis are used while the others are set at zero, except the corner of the PML domains (Collino and Tsogka, 2001). For example, the four sides of the PML layer (not including the corners) take $d_x$ or $d_z$ depending on the direction and the four corners take both $d_x$ and $d_z$ in the above 2D model.

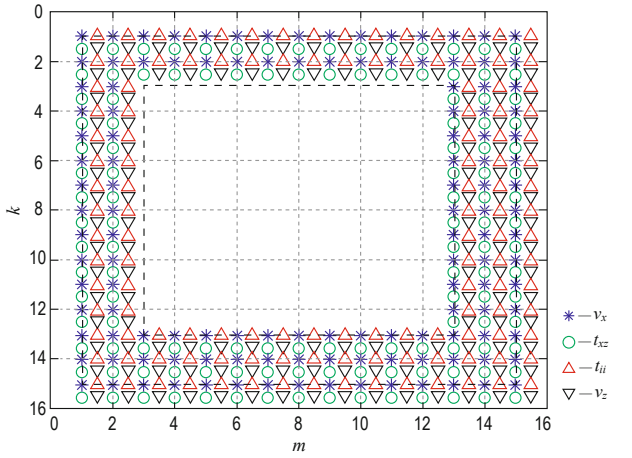


**Fig. 2 Schematicof a 2D model with a PML and a rectangular computational domain.**

$v_x$ and $v_z$ are the velocity in horizontal and vertical direction, respectively. $t_{ii}$ and $t_{xz}$ are the normal and shear stress.

## Multi-axial perfectly matched layer (M-PML)

Meza-Fajardo and Papageorgiou (2008) analyzed the numerical stability of SPML and introduced a modified version, M-PML, in which damping in different directions are coupled. Again, taking the $x$ direction as an example, the damping profile consists of three parts: $d_x^x(x)$, which can be derived from SPML, $d_y^x(x)$, and $d_z^x(x)$, which are the corrections in the $y$ and $z$ directions, respectively. Here, the subscript $x$, $y$, and $z$ are the normal directions and the superscript $x$ is the damping direction, where $d_x^y(x) = p_{yx}\, d_x^x(x)$, $d_x^z(x) = p_{zx}\, d_x^x(x)$; $p_{yx}$ and $p_{zx}$ are the correction coefficients that can be tuned according to specific cases. According to Meza-Fajardo and Papageorgiou (2008), a $p_0 \in [0, 1]$ could find where the MPML is stable for all $p > p_0$. However, the reflectivity

will be increased when the stability is improved.

In other words, the wave in the $x$ direction will be damped in the $x$ direction and will also be damped in the other two directions ($y$ and $z$). Therefore, the damping coefficients of M-PML are:

$$d_x = d_x^x(x) + d_x^y(y) + d_x^z(z),$$
$$d_y = d_y^x(x) + d_y^y(y) + d_y^z(z),$$
$$d_z = d_z^x(x) + d_z^y(y) + d_z^z(z). \quad (7)$$

In fact, Martin et al. (2010) made the case that the M-PML should not be considered a PML, as the theoretical reflection coefficient for an infinite PML is not exactly zero in this approach. It is just a modification of a sponge and the reflection coefficients are not zeros, even for differential formulations (Dmitriev and Lisitsa, 2011). The M-PML is a brutal-force approach that allows anisotropy and high contrasts to be dealt with (Meza-Fajardo and Papageorgiou, 2008).

## Non-splitting perfectly matched layer (NPML)

To simplify the implementation of classic PML, Wang and Tang (2003b) introduced the non-splitting PML (NPML), in which a trapezoidal rule is applied to calculate the convolutions in the PML formulation. For example, equation (3) can be transformed into the time domain using the inverse Fourier transforms as follows:

$$\rho\frac{\partial v_x}{\partial t} = F^{-1}\left(\frac{1}{S_x(x)}\right) * \frac{\partial \sigma_{xx}}{\partial x} + F^{-1}\left(\frac{1}{S_y(y)}\right) * \frac{\partial \sigma_{yx}}{\partial y} + F^{-1}\left(\frac{1}{S_z(z)}\right) * \frac{\partial \sigma_{zx}}{\partial z}, \quad (8)$$

where

$$F^{-1}\left(\frac{1}{S_x(x)}\right) * \frac{\partial \sigma_{xx}}{\partial x} = \frac{\partial \sigma_{xx}}{\partial x} - d_x(x)\int_0^T e^{-d_x(x)(T-t)}\frac{\partial \sigma_{xx}}{\partial x}dt.$$

The two other convolution expressions will have the same form. Therefore, the formulation of velocity in $x$ direction will be:

$$\rho\frac{\partial v_x}{\partial t} = \frac{\partial \sigma_{xx}}{\partial x} - d_x(x)\int_0^T \exp\left[-d_x(x)(T-t)\right]\frac{\partial \sigma_{xx}}{\partial x}dt + \frac{\partial \sigma_{yx}}{\partial y} - d_y(y)\int_0^T \exp\left[-d_y(y)(T-t)\right]\frac{\partial \sigma_{yx}}{\partial y}dt + \frac{\partial \sigma_{zx}}{\partial z} - d_z(z)\int_0^T \exp\left[-d_z(z)(T-t)\right]\frac{\partial \sigma_{zx}}{\partial z}dt. \quad (9)$$

Taking the time step as $\Delta t$, and the time in $i$ steps as $T = i\Delta t$, then formulation (9) should be as follows:

$$\rho\frac{\partial v_x}{\partial t} = \frac{\partial \sigma_{xx}}{\partial x} - d_x(x)\int_0^{i\Delta t} \exp\left[-d_x(x)(i\Delta t-t)\right]\frac{\partial \sigma_{xx}}{\partial x}dt + \frac{\partial \sigma_{yx}}{\partial y} - d_y(y)\int_0^{i\Delta t} \exp\left[-d_y(y)(i\Delta t-t)\right]\frac{\partial \sigma_{yx}}{\partial y}dt + \frac{\partial \sigma_{zx}}{\partial z} - d_z(z)\int_0^{i\Delta t} \exp\left[-d_z(z)(i\Delta t-t)\right]\frac{\partial \sigma_{zx}}{\partial z}dt. \quad (10)$$

The time discrete form of equation (10) is as follows:

$$v_x^{i+1/2} = v_x^{i+1/2} + \frac{\Delta t}{\rho}\left(\frac{\partial t_{xx}}{\partial x} + \frac{\partial t_{yx}}{\partial y} + \frac{\partial t_{zx}}{\partial z}\right),$$
$$v_x^{i+1/2} = v_x^{i+1/2} - P_{xx}^i - P_{yx}^i - P_{zx}^i, \quad (11)$$

where

$$P_{xx}^i = d_x(x)\int_0^{i\Delta t} e^{-d_x(x)(i\Delta t-t)}\frac{\partial t_{xx}}{\partial x}dt,$$
$$P_{yx}^i = d_y(y)\int_0^{i\Delta t} e^{-d_y(y)(i\Delta t-t)}\frac{\partial t_{yx}}{\partial y}dt,$$
$$P_{zx}^i = d_z(z)\int_0^{i\Delta t} e^{-d_z(z)(i\Delta t-t)}\frac{\partial t_{zx}}{\partial z}dt.$$

The trapezoidal rule can be used for the numerical approximation of the integrations above. For example:

$$P_{xx}^i = d_x(x)P_{xx}^{i-1} + \frac{1}{2}\Delta t d_x(x)\left(e^{-d_x(x)\Delta t}\left.\frac{\partial t_{xx}}{\partial x}\right|^{(i-1)} + \left.\frac{\partial t_{xx}}{\partial x}\right|^{i}\right),$$

in which the auxiliary function is introduced to obtain the integration with second-order time accuracy.

## Complex frequency-shifted perfectly matched layer (CFS-PML)

Ineffective absorption of evanescent waves and instability in long duration simulations have been reported in electromagnetic wave simulations (Berenger, 1997) by FDTD with conventional PML (Berenger, 1994). To address the limitations of conventional PML, many scholars have devoted a great deal of effort to the theory and practice of modifying PML. Kuzuoglu and

Mittra (1996) analyzed the causality of conventional PML and found that the conventional stretch factor does not meet the causality. They introduced complex frequency-shifted (CFS) PML, where they used a modifying factor $S = 1 + d/(1+i\omega)$.

Furthermore, the conventional PML method no longer applies when the wavenumber is a pure imaginary number, such as in the case of evanescent waves and guided waves. For example, if $k_x$ is a negative imaginary number (Skelton et al., 2007), it can be replaced by $k_x = -ik$ (where $k$ is a real number). The plane wave solution in the $x$ direction will become $\exp(-ik_x x)\exp(ikd_x x/\omega)$. The factor $\exp(ikxd_x/\omega)$ will make the signal oscillate without attenuation. In comparison, the solution with the modified factor by Kuzuoglu and Mittra (1996) will be $\exp(-ik_x x)\exp(ik\omega d_x x/(1+\omega^2))\exp(-kxd_x/(1+\omega^2))$, in which the factor $\exp(-kxd_x/(1+\omega^2))$ can exponentially attenuate the energy with increasing distance.

To absorb guide waves and evanescent waves efficiently, Roden and Gendney (2000) proposed a general stretch factor $\mathbf{S} = \beta + d/(\alpha+i\omega)$ for CFS-PML, where $\alpha$ is a frequency-shifted factor and $\beta$ is a scaling factor. Komatitch and Martin (2007) used a recursive convolutional method to implement the CFS-PML with FDTD. Taking equation (7) as an example, the inverse Fourier transform of 1/S is expressed as follows:

$$\hat{S} = F^{-1}\left(\frac{1}{S}\right) = \frac{\delta(t)}{\beta} - \frac{d}{\beta^2}F^{-1}\left[\frac{1}{\alpha + \frac{d}{\beta} + i\omega}\right]$$
$$= \frac{\delta(t)}{\beta} - \frac{d}{\beta^2}H(t)e^{-(\alpha+d/\beta)t}. \quad (12)$$

Then equation (7) is as follows:

$$\rho\frac{\partial v_x}{\partial t} = \hat{S}_x * \frac{\partial \sigma_{xx}}{\partial x} + \hat{S}_y * \frac{\partial \sigma_{yx}}{\partial y} + \hat{S}_z * \frac{\partial \sigma_{zx}}{\partial z}. \quad (13)$$

The recursive convolutional method that is used to realize equation (13) has only second-order accuracy (Martin et al., 2010). To keep PML time accuracy the same as the computational domain, Zhang and Shen (2010) used the auxiliary differential equations (ADE) method to attain higher-order time accuracy. See Zhang and Shen (2010) for more details.

Table 2 compares the different PML methods to illustrate how CFS-PML differs from the others.

In general, the damping profile is chosen as a polynomial function. Here, we follow Collino's equation (2001) for damping in the $x$ direction:

$$d_x = d_0\left(\frac{l_x}{L}\right)^n, \quad (14)$$

where $l_x$ is the distance from the PML interior interface for the location in the PML domain, $n$ is 2, $d_0$ is the maximum value of $d$, which can be obtained from Collino and Tsogka (2001), and $L$ is the thickness of the PML layer.

**Table 2 Summary of PML methods**

| | SPML | M-PML | NPML | CFS-PML |
|---|---|---|---|---|
| $\alpha$ | 0 | 0 | 0 | Non-zero |
| $\beta$ | 1 | 1 | 1 | Variable |
| $d_x$ | $d_x^x(x)$ | $d_x^x(x)$, $d_x^y(x)$, $d_x^z(x)$ | $d_x^x(x)$ | $d_x^x(x)$ |
| Convolution | No | No | Yes | Yes |

The value of $\alpha$ and $\beta$ in CFS-PML are usually given by the following polynomials (Komatitsch and Martin, 2007):

$$\beta_x = 1 + (\beta_0 - 1)\left(\frac{l_x}{L}\right)^m, \quad (15)$$

$$\alpha_x = \alpha_0\left(1 - \left(\frac{l_x}{L}\right)^p\right), \quad (16)$$

where $m$ and $p$ are 2 and 1, respectively, and $\alpha_0$ and $\beta_0$ are the maximum values of $\alpha$ and $\beta$.

# Numerical results and discussion

## Results of 2D FDTD LWD acoustic simulation with different PML methods

To quickly determine the applicability of the different PML methods in the ALWD model, we implemented the four different PML methods in FDTD in the 2D LWD monopole case for the model shown in Figure 1c. For the 2D ALWD model, the FD code in the cylindrical coordinate system is often used to describe the simulation. However, 2D simulations in the Cartesian coordinate system could also demonstrate the fluid-solid interface problem and the applicability of the PML methods for the ALWD case. We chose the FD code in the Cartesian coordinate system for the convenience, although it is just a profile not a real borehole.

## Stability of PML for LWD acoustic simulation

For the sandstone formation case in Table 1, the staggered grid FDTD scheme was used with fourth-order accuracy in space and second-order in time (Tao et al., 2008). The model was discretized into 123 by 334 grids along the $x$ and $z$ direction, respectively. The grid spacing was 9 mm and the time step was 0.9 μs. The PML layer thickness was 20 grids. A monopole source was applied and the source time function was a Ricker wavelet with central frequency $f_c$ of 10 kHz. $d_0$ and $\alpha_0$ were chosen as 1 and $\pi f_c$ respectively. The results are shown in Figure 3.

For the case of SPML (Figure 3a), it was possible to identify the drill collar wave, shear (S) wave, and Stoneley wave arrivals from their arrival times. Furthermore, the artificial reflection from the model boundaries (dashed black line) was visible, which was a reflected Stoneley wave from the top boundary in the borehole (its velocity was 1389 $m \cdot s^{-1}$) as calculated by the time semblance method (Kimball and Marzetta, 1984). The simulation becomes unstable after 10 ms, indicating the ill-posed nature of the SPML scheme in the LWD case.

Figure 3b shows the result of M-PML with correction coefficients $p_{zx}$ and $p_{xz}$ taken as 0.1. The reflection artifacts were still visible, but the instability issue was improved to some extent (it appeared after 13 ms and without the high-frequency component), which indicates that the M-PML can be used to simulate a longer signal if the correction coefficients are suitable. If we could find a suitable value for $p_0$ between 0 and 1, the simulation would be stable when all values of $p$ are greater than $p_0$. However, the reflectivity would increase.

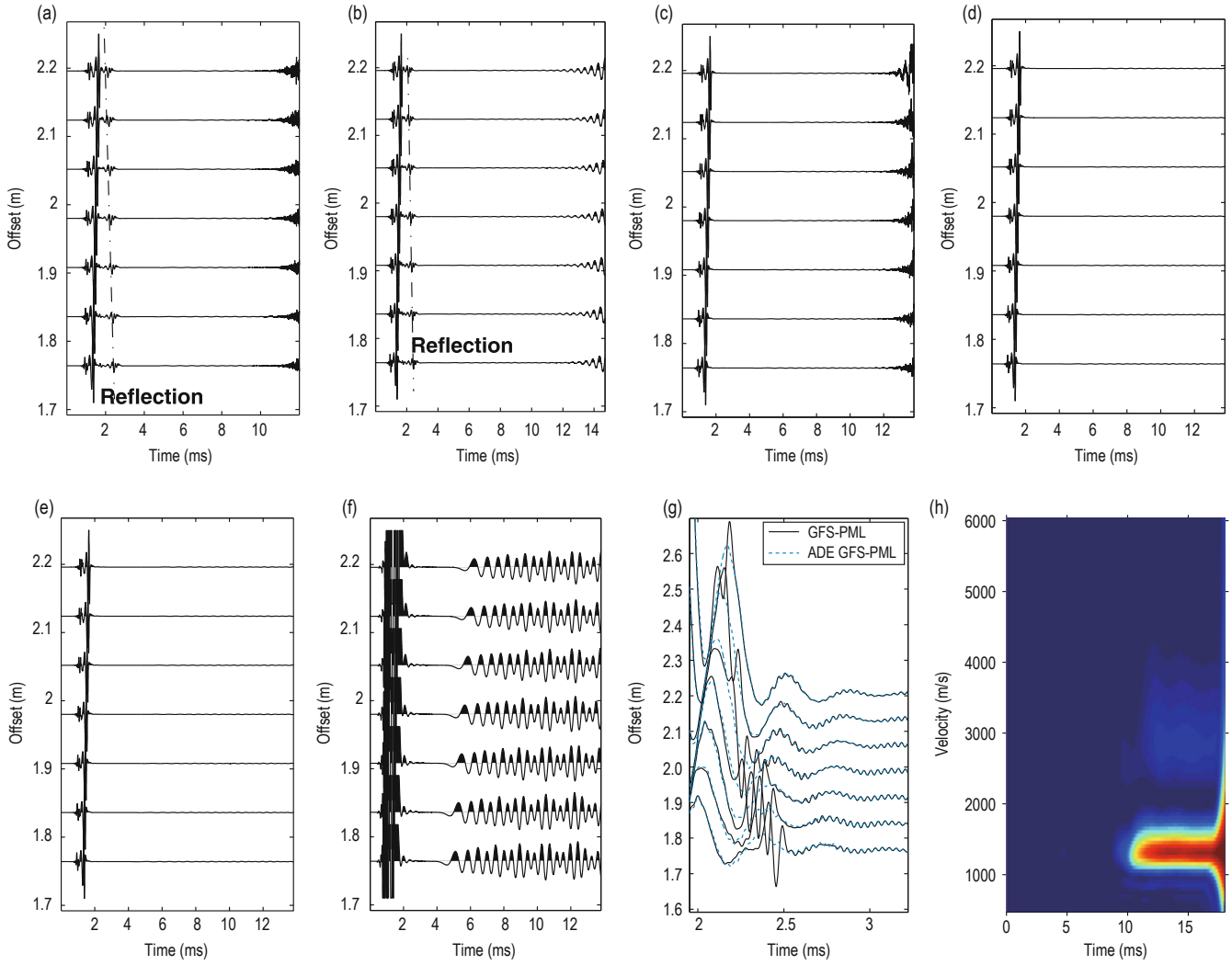


**Fig.3 Waveform of array receivers in the LWD case.**

Results of (a) SPML, (b) M-PML, (c) NPML, (d) CFS-PML ($\beta_0 = 1$), and (e) ADE CFS-PML ($\beta_0 = 7$). (f) Waveform of (e) zoomed in by 100 times. (g) Comparison of (d) and (e). (h) Velocity–time analysis of the array waveform after 4 ms of (f).

If we want to obtain good simulation results, we need to find a coefficient that provides a balance between stability and reflectivity.

Figure 3c shows the result of NPML. Comparing Figure 3a with 3c, NPML (Figure 3c) is superior to SPML and M-PML in suppressing the reflected Stoneley wave. However, the intrinsic instability of NPML (after 12 ms in Figure 3c) in the LWD case indicates that it is not suitable for large simulation time.

We implemented the CFS-PML (Figure 3d) with $\alpha_0 = \pi f_c$ and $\beta_0 = 1$. From Figure 3d, we found that CFS-PML can attenuate the reflected wave from the boundary and remain stable for long simulation time. CFS-PML appears to be the most effective implementation of the four in terms of stability and absorbance efficiency. We also implemented the ADE CFS-PML method, which can be easily used for higher-order time accuracy, such as a fourth-order Runge-Kutta time-marching scheme (Zhang and Shen, 2010). In this case, we chose the $\alpha_0 = \pi f_c$ and $\beta_0 = 1$ then changed $\beta_0$ to 7 (according to Zhang and Shen (2010)). The same result as Figure 3d is obtained with $\beta_0 = 1$. Figure 3e shows the case of the ADE CFS-PML with $\beta_0 = 7$. Although it looks as though it has almost the same effect as CFS-PML, the difference

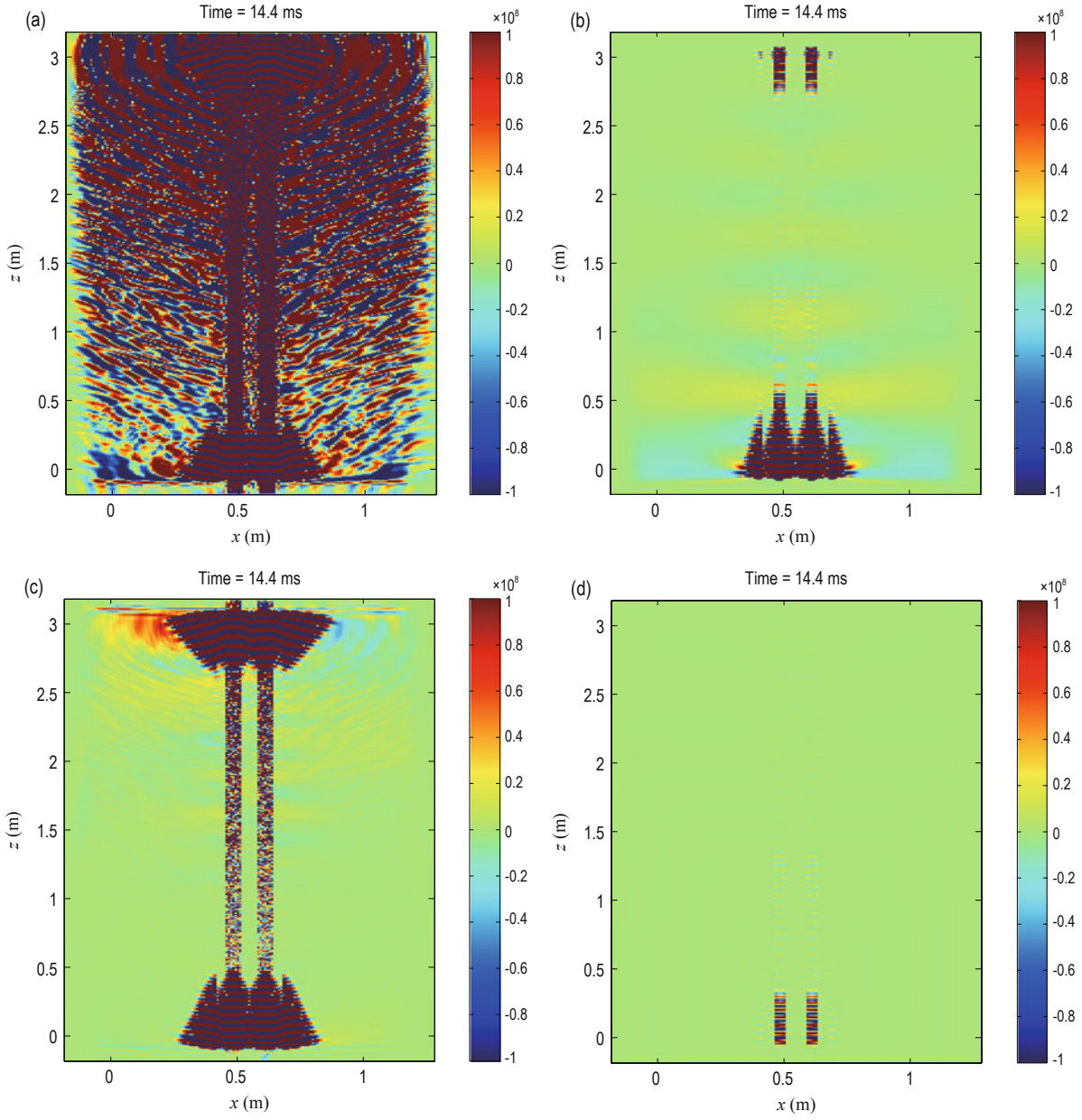


**Fig.4 Snapshot of wave field of 2D LWD acoustic case at 14.4 ms.**
Results of (a) SPML, (b) M-PML, (c) NPML, and (d) CFS-PML.

is found by comparison with Figure 3g, in which the reflection from the boundary can be eliminated better with a suitable value of $\beta_0$. The coda wave arrives after 4 ms in Figure 3e, which is zoomed in by 100 times in Figure 3f. These arrivals are reflected Stoneley waves as dominantly time semblance (Figure 3h). In the LWD FDTD simulations, PML artifacts are guided waves (e.g., Stoneley wave) generated at boundaries.

Figure 4 shows the wavefield snapshots of FDTD simulations in the 2D LWD with different PML methods. The PML domains are also shown in the snapshots. The source location in the z direction is 0.45 m. Here, we can see that the numerical instability and reflected wave are generated at the fluid–steel interface. The CFS-PML gets the best results, although there are still some unabsorbed guided waves. M-PML is the second best PML of the four methods.

## Parameter optimization of CFS-PML in 3D FDTD LWD acoustic simulations

The effects of CFS-PML parameters on the absorption efficiency based on totally homogenous models have been discussed previously (Komatitsch and Martin, 2007; Zhang and Shen, 2010). Here, we optimized the parameters specifically for some typical 3D LWD acoustic simulations (monopole cases for limestone formation, sandstone formation, and mudstone formation, shown as Figure 1a, and a quadrupole case for mudstone formation, shown as Figure 1b). The computational domain for the 3D model is 30 cm by 30 cm by 20 cm (shown in Figure 1). The media parameters and borehole geometry are defined in Table 1. The space grid size was 5 mm, the time step was 0.38 μs in the limestone case, and the total simulation time was 2 ms. There were 6 points per dominant wavelength and the central frequency was 10 kHz for the monopole mode and 3 kHz for the quadrupole mode. About 3000 simulations for each case are performed (each simulation takes ~10 min by parallel computer) using different PML parameter combinations. Here, $d_0$, $\alpha_0$, $\beta_0$ and L are considered. A large model was chosen as a reference model, in which no reflected energy from the boundaries appears in the first 2 ms time window. The global relative error was defined as:

$$E_g = \frac{\sum_t \left| P_{PML}(t) - P_{ref}(t) \right|}{\sum_t \left| P_{ref}(t) \right|}, \qquad (17)$$

where $E_g$ is the global error of a given PML model, $P_{PML}$ and $P_{ref}$ are the pressure fields of the PML model and reference model respectively, and $t$ is time. The global errors are shown in the following figures, for different parameters, $d_0$, $\alpha_0$, $\beta_0$ and L. Figures 5 and 6 show the monopole case for sandstone formation. As shown in Figure 5, the global error changes with $d_0$. The minimum global error is <1% with one $d_0$, which is the best value in the simulations. This result differs from the result of Zhang and Shen (2010) due to the layered homogeneous model in the LWD case. We also find that the optimal value of $\beta_0$ is between 10 and 27, and the best combination of $\alpha_0$ and $\beta_0$ is ~$1.5\pi f_c$ and 20, respectively, from Figure 5b. These values deviate from the empirical a formula for $\beta_0$ according to Zhang and Shen (2010), which gives values of 39.067 for the monopole case in a sandstone formation. Therefore, it seems that the empirical formula of $\beta_0$ should be modified for layered homogeneous models such as the LWD case.

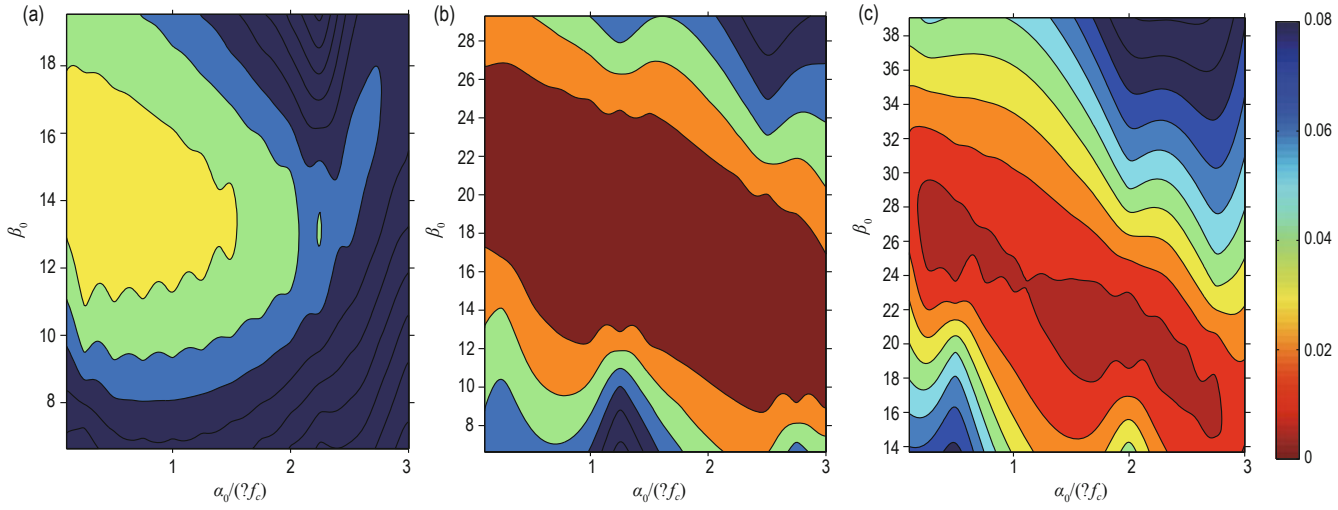

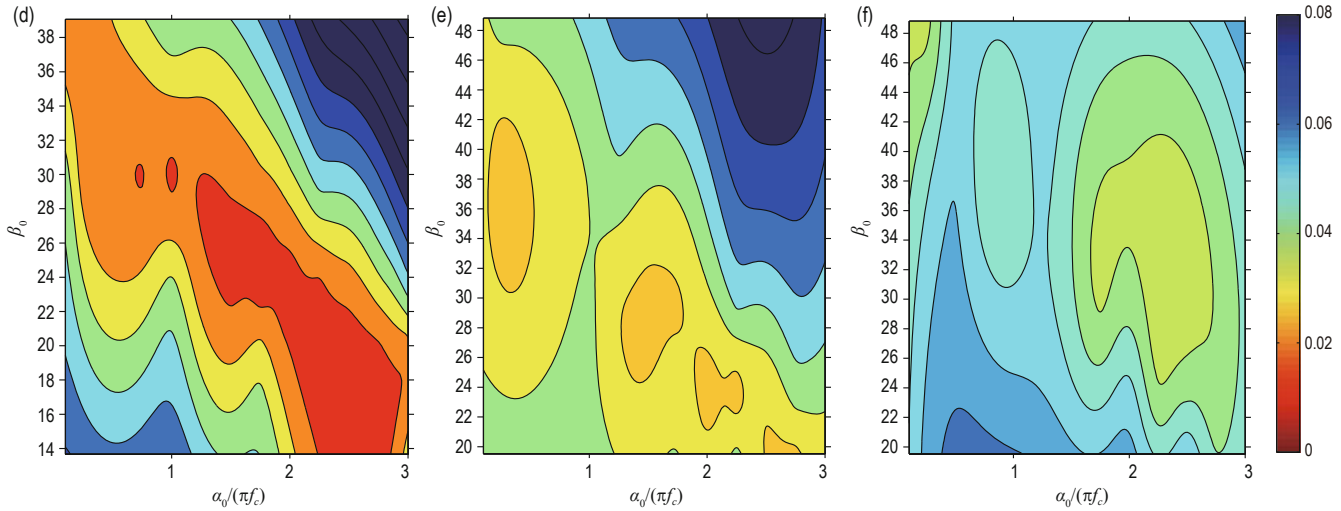


**Fig.5 Contours of global error with $\alpha_0$, $\beta_0$, and d0variation ($L$ = 10).**
Contours of global error as a function of $\alpha_0$ and $\beta_0$ with (a) 0.5 $d_0$, (b) $d_0$, (c) 1.5 $d_0$, (d) 2$d_0$, (e) 2.5$d_0$, and (f) 3$d_0$.

The effect of the thickness of the PML on global error with one $d_0$ is shown in Figure 6. Combining Figure 6 with Figure 5(b), we found that the global error decreased as L increased, and the range of optimal $\alpha_0$ and $\beta_0$ became larger. By increasing the PML thickness to 20 grid points, we obtained a global error of < 5‰ for a large range of $\alpha_0$ and $\beta_0$. This indicated the overall high level of performance of CFS-PML.

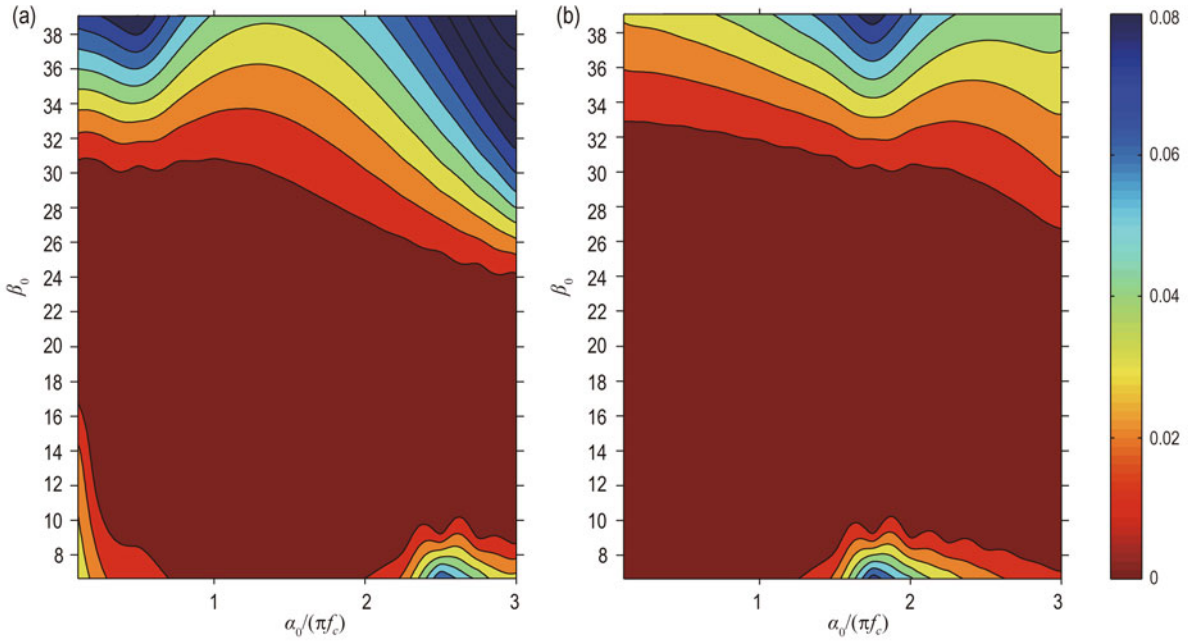


**Fig.6 Contours of global error with $\alpha_0$, $\beta_0$, and L variation.**
Contours of global error as a function of $\alpha_0$, and $\beta_0$ with L equal to (a) 20 and (b) 30.

To test the CFS-PML for a wider range of formation properties, we also looked at results for a monopole source for a limestone formation and mudstone formation, and a quadrupole source for a mudstone formation. Figure 7 shows the contours of global error with $\alpha_0$ and $\beta_0$ variation, in which a 10 grid points PML thickness and one $d_0$ are considered. For the monopole case in mudstone (Figure 7a), we clearly found that the global error will be >2% for a large range of $\alpha_0$ and $\beta_0$, and the optimal value of $\beta_0$ is between ~15 and

40 (43.3 for monopole case in limestone according to Zhang and Shen (2010) for totally homogeneous media). Similarly, we found the optimal value of $\alpha_0$ and $\beta_0$ for the monopole and quadrupole cases in mudstone formation from Figures 7b and 7c. The optimal value of $\beta_0$ was from ~10 to 17 (39 according to Zhang and Shen (2010) for totally homogeneous media) and $\alpha_0$ had two optimal areas: ~$1.2\pi f_c$ to $1.4\pi f_c$ and $1.7\pi f_c$ to $2\pi f_c$ for the monopole case in the mudstone formation. The optimal value of $\alpha_0$ is from ~20 to 40 (130 according to Zhang and Shen ( 2010) for totally homogeneous media) for the quadrupole case in the mudstone formation.

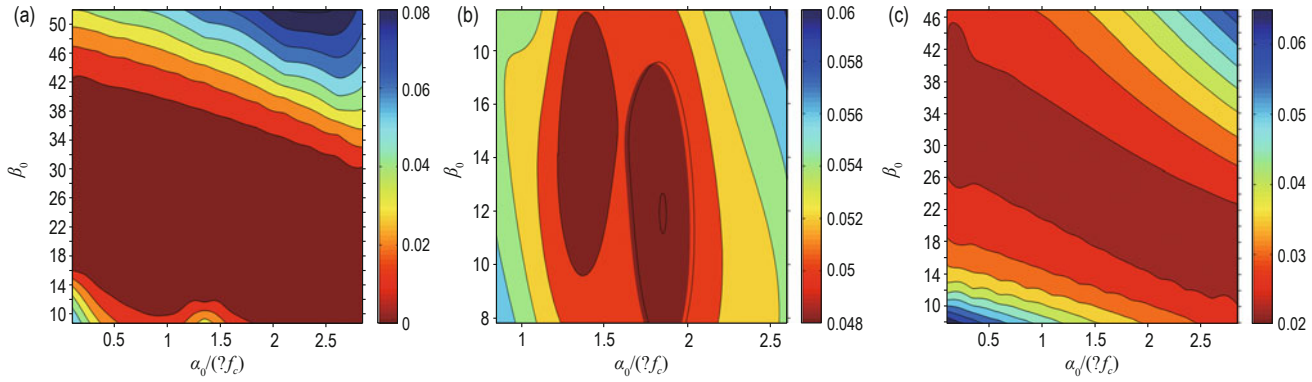


**Fig.7 Contours of global error with $\alpha_0$ and $\beta_0$ variation ($d_0$ = 1, $L$ = 10).**
(a) Contours of global error as a function of $\alpha_0$ and $\beta_0$ (a) in the monopole case for limestone, (b) in the monopole case for mudstone, and (c) $\beta_0$ in the quadrupole case for mudstone.

## Conclusions

Four kinds of PML were implemented with FDTD in a 2D acoustic LWD simulation. The simulation results indicated that NPML and CFS-PML can more efficiently absorb the guided wave reflections from the computational boundaries than SPML and M-PML. For long duration simulations, numerical instability was observed in SPML, M-PML, and NPML, though M-PML can improve the stability to some extent by fine tuning of the parameters. Among all methods, CFS-PML was the best choice for acoustic LWD FDTD simulation for both efficient absorption and numerical stability.

The effects of CFS-PML parameters on the absorbance efficiency were investigated based on thousands of 3D simulations. For typical LWD cases, the best maximum value of the quadratic damping profile (d) is one $d_0$. The optimal parameter space for the maximum value of the linear frequency-shifted factor ($\alpha_0$) and the scaling factor ($\beta_0$) depended on the thickness of the PML layer. For typical formations, if the PML thickness is 10 grid points, the global error can be reduced to <1% using the optimal PML parameters, and the error will decrease as the PML thickness increases. The range of optimal values of $\alpha_0$ and $\beta_0$ are given for typical formations in the LWD acoustic situation.

## References

Alterman, Z., and Karal, F. C., 1968, Propagation of elastic waves in layered media by finite difference methods: Bulletin Of The Seismological Society Of America, **58**, 367 – 398.

Aron, J., Chang, S. K., Codazzi, D., Dworak, R., Hsu, K., Lau, T., Minerbo, G., and Yogeswaren, E, 1997, Real-time sonic logging while drilling in hard and soft rocks: SPWLA 38th Annual Logging Symposium, Paper HH.

Berenger, J, 1994, A perfectly matched layer for the absorption of electromagnetic waves: Journal of Computational Physics, **114**, 185 – 200.

Berenger, J. P., 1997, Improved PML for the FDTD solution of wave-structure interaction problems: IEEE Transactions on Antennas and Propagation, **45**, 466 – 473.

Bouchon, M., and Aki, K., 1977, Discrete wave-number representation of seismic-source wave fields: Bulletin of the Seismological Society of America, **67**, 259 – 277.

Byun, J., and Toksoz, M. N., 2003, Analysis of the acoustic wave fields excited by the logging-while-drilling (LWD) tool: Geosytem Eng., **6**, 19 – 25.

Carcione, J. M., 1994, The wave equation in generalized coordinates: Geophysics, **59**, 1911 – 1919.

Cerjan, C., Kosloff, D., Kosloff, R., and Reshef, M., 1985, A nonreflecting boundary condition for discrete acoustic

and elastic wave equations: Geophysics, **50**, 705 – 708.

Chen, Y., and Chew, W. C.,and Liu, Q., 1998, A three-dimensional finite difference code for the modeling of sonic logging tools: Journal of the Acoustical Society of America, **103**, 702 – 712.

Cheng, C. H., and Toksoz, M. N., 1981, Elastic wave propagation in a fluid-filled borehole and synthetic acoustic logs: Geophysics, **46**, 1042 – 1053.

Cheng, N., 1994, Borehole Wave Propagation in Isotropic and Anisotropic Media:Three-Dimensiona Finite Difference Approach: PhD thesis, Massachusetts Institute of Technology, USA.

Chew, W. C., and Liu, Q. H., 1996, Perfectly matched layers for elastodynmics:A new absorbing boundary condition: J.Comp.Acoust., **4**, 341 – 359.

Chew, W. C., and Weedon, W.H., 1994, A 3D perfectly matched medium from modified Maxwell's equations with stretched coordinates: Microwave Optical Tech. Letters, **7**, 599 – 604.

Clayton, R., and Engquist, B., 1977, Absorbing boundary conditions for acoustic and elastic wave equations: Bulletin of the Seismological Society, **67**, 1529 – 1540.

Cohen, G., Joly, P., and Tordjman, N., 1993, Construction and analysis of higher-order finite elements with mass lumping for the wave equation: Conference Construction and Analysis of Higher-order Finite Elements with Mass Lumping for the Wave Equation, 152 – 160.

Collino, F., and Tsogka, C., 2001, Application of the perfectly matched absorbing layer model to the linear elastodynamic problem in anisotropic heterogeneous media: Geophysics, **66**, 294 – 307.

Dmitriev, M., and Lisitsa, V., 2011, Application of M-PML reflectionless boundary conditions to the numerical simulation of wave propagation in anisotropic media. Part I: Reflectivity: Numerical Analysis and Applications, **4**, 271 – 280.

Guan, W., Hu H., and He, X., 2009, Finite-difference modeling of the monopole acoustic logs in a horizontally stratified porous formation: J. acoust. Soc. Am., **125**(4), 1942 – 1950.

Higdon, R. L., 1990, Radiation boundary conditions for elastic wave propagation: SIAM Journal on Numerical Analysis,27, 831-869.

Huang, X., 2003, Effects of tool positions on borehole acoustic measurements: a stretched grid finite difference approach: PhD thesis, Massachusetts Institute of Technology, USA.

Kawase, H., 1988, Time-domain response of a semi-circular canyon for incident SV, P and Rayleigh waves calculated by the discrete wavenumber boundary element method: Bulletin of the Seismological Society of America, **78**, 1415 – 1437.

Kimball, C. V., and Marzetta, T. L., 1984, Semblance processing of borehole acoustic array data: Geophysics, **49**, 274 – 281.

Komatitsch, D., and Martin, R., 2007, An unsplit convolutional perfectly matched layer improved at grazing incidence for the seismic wave equation: Geophysics, **72**, SM155 – SM167.

Kurkjian, A., and Chang, S. K., 1986, Acoustic multipole sources in fluid filled boreholes: Geophysics, **51**, 148 – 163.

Kuzuoglu, M., and Mittra, R., 1996, Frequency dependence of the constitutive parameters of causal perfectly matched anisotropic absorbers: Microwave and Guided Wave Letters, IEEE, **6**, 447 – 449.

Lysmer, J., and Drake, L. A., 1972, A finite element method for seismology, in B. Alder, S. Fernbach, and B. A. Bolt, eds: Methods in computational physics, 181 – 216.

Madariaga, R., 1976, Dynamics of an expanding circular: Bulletin of the Seismological Society of America, **66**, 639 – 666.

Marfurt, K. J., 1984, Accuracy of finite-difference and finite-element modeling of the scalar and elastic wave equations: Geophysics, **49**, 533 – 549.

Martin, R. D., Komatitsch, S. D., Gedney, and Bruthiaux, E., 2010, A high-order time and space formulation of the unsplit perfectly matched layer for the seismic wave equation using auxiliary differential equations (ADE-PML): CMES, **56**, 17 – 40.

Matuszyk, P. J., and Torres-Verdin, C., 2011, HP-adaptive multi-physics finite-element simulation of wireline borehole sonic waveforms: SEG Technical Program Expanded Abstracts, **30**, 444 – 448.

Meza-Fajardo, K. C., and Papageorgiou, A. S., 2008, A nonconvolutional, split-field, perfectly matched layer for wave propagation in isotropic and anisotropic elastic media: Stability analysis: Bulletin of the Seismological Society of America, **98**, 1811 – 1836.

Roden, J. A., and Gedney, S. D., 2000, Convolutional PML (CPML): An efficient FDTD implementation of the CFS-PML for arbitrary media: Microwave and Optical Technology Letters, **27**, 334 – 338.

Schmitt, D., and Bouchon, M., 1985, Full-wave acoustic logging: Synthetic micro seismogram and frequency-wave number analysis: Geophysics, **50**, 1756 – 1778.

Skelton, E. A., Adams, S. D. M., and Craster, R.V., 2007, Guided elastic waves and perfectly matched layers: Wave Motion, **44**, 573 – 592.

Smith, W. D., 1974, A nonreflecting plane boundary for wave propagation problems: Journal of Computational Physics, **15**, 492 – 503.

Sochacki, J., Kubichek, R., George, J., Fletcher, W. R., and Smithson, S., 1987, Absorbing boundary conditions and

surface waves: Geophysics, **52**, 60 – 71.

Tao, G., He, F., Wang, B., Wang, H., and Chen, P., 2008, Study on 3D simulation of wave fields in acoustic reflection image logging: Science China (Earth Sciences Version), **51**(S2), 186 – 194.

Tessmer, E., and Kosloff, D., 1994, 3-D elastic modeling with surface topography by a Chebyshev spectral method: Geophysics, **59**, 464 – 473.

Virieux, J., 1984, SH wave propagation in heterogeneous media: Velocity-stress finite-difference method: Geophysics, **49**, 1933 – 1957.

Virieux, J., 1986, P-SV wave propagation in heterogeneous media: Velocity-stress finite-difference method: Geophysics, **51**, 889 – 901.

Wang, H., and Tao, G., 2011, Wavefield simulation and data-acquisition-scheme analysis for LWD acoustic tools in very slow formations: Geophysics, **76**, E59 – E68.

Wang, H., Tao, G., Wang, B., Li, W., and Zhang, X., 2009, Wave field simulation and data acquisition scheme analysis for LWD acoustic tool: Chinese J. Geophysics (In Chinese), **52**, 2402 – 2409.

Wang, H., Tao, G., Zhang, K., and Li, J., 2012, Numerical simulations for acoustic reflection imaging with FDM and FEM: EAGE Technical Program Expanded Abstracts, E041.

Wang, H., Tao, G., and Zhang, K., 2013, Wavefield simulation and analysis with the finite-element method for acoustic logging while drilling in horizontal and deviated wells: Geophysics, **78**(6), D525 – D543.

Wang, T., and Tang, X., 2003a, Investigation of LWD quadrupole shear measurement in real environments: SPWLA 44th Annual Logging Symposium, Paper KK.

Wang, T., and Tang, X., 2003b, Finite-difference modeling of elastic wave propagation: A nonsplitting perfectly matched layer approach: Geophysics, **68**, 1749 – 1755.

He, X., Hu, S., and Wang, X., 2013, Finite difference modeling of dipole acoustic logs in a poroelastic formation with anisotropic permeability: Geophys. J. Int. **192**(1), 359 – 374.

Zhang, W., and Shen, Y., 2010, Unsplit complex frequency-shifted PML implementation using auxiliary differential equations for seismic wave modeling: Geophysics, **75**, T141 – T154.

Zhu, J., 1999, A transparent boundary technique for numerical modeling of elastic waves: Geophysics, **64**, 963 – 966.

**Hua Wang** is a Postdoctoral Fellow at China University of Petroleum (Beijing). He received a BS degree, MS degree and PhD. degree in applied geophysics from China University of Petroleum in 2005, 2008, and 2012, respectively. And he was a visiting student at Earth Resource Lab of MIT during Sept.2010 and Oct. 2011 under the guidance of Dr. Mike Fehler and Dr. Dan Burns. He was a visiting research scientist at University of Science and Technology of China focused on micro-seismicity during Nov. 2012 and July. 2013. The research interests of him are well logging, and micro-seismicity.